The LTB_4-BLT1 signaling axis coordinates actomyosin dynamics and β-2 Integrin trafficking to drive intravascular neutrophil response to infection

Bhagawat C. Subramanian[1], Nicolas Melis[1], Desu Chen[1], Weiye Wang[1], Devorah Gallardo[2], Roberto Weigert[1]* and Carole A. Parent[1,3]*

[1] Laboratory of Cellular and Molecular Biology, Center for Cancer Research, National Cancer Institute, NIH, Bethesda, MD 20892, USA

[2] Laboratory Animal Sciences Program, Leidos Biomedical Research, National Cancer Institute, NIH, Bethesda, MD 20892, USA

[3]Department of Pharmacology, University of Michigan, Ann Arbor, MI 48109, USA

***Co-Corresponding senior authors**

ABSTRACT

The eicosanoid Leukotriene B_4 (LTB_4) relays chemotactic signals to direct neutrophil interstitial migration through its receptor, BLT1. However, whether the LTB_4-BLT1 axis relays signals during intravascular neutrophil response has not been addressed. Here, we report that LTB_4 produced by neutrophils acts as an autocrine/paracrine signal to drive neutrophil recruitment, arrest, and extravasation during infection in living mice. Using Intravital Subcellular Microscopy (ISMic), we reveal that LTB_4 elicits sustained cell polarization and adhesion response during neutrophil arrest *in vivo*. Specifically, LTB_4 signaling coordinates the dynamic redistribution of non-muscle Myosin IIA (NMIIA) and β_2-integrin (Itgb2), whose retention at the cell surface facilitates neutrophil arrest. Notably, we also found that inhibition of the machinery regulating exosomes release from the cell blocks the autocrine/paracrine LTB_4-dependent extravasation response. Overall, our study reveals a critical function for LTB_4 in promoting neutrophil communication in the vasculature during early inflammation response.

Keywords – Neutrophils, infection, LTB_4, BLT1, intravital microscopy, actomyosin, integrin, adhesion, extravasation, exosomes, autocrine, paracrine.

INTRODUCTION

Neutrophils are the first mediators of innate immune responses[1,2,3]. As they start their journey to reach sites of inflammation/injury, neutrophils in blood vessels respond by rolling on and adhering to the endothelium, and extravasating into the interstitium (transendothelial migration or diapedesis)[2,4], where they migrate directionally by sensing chemotactic gradients. Neutrophils respond to primary chemoattractants, such as formylated peptides and Complement 5a (C5a), by producing the lipid mediator LTB_4 through the activity of the 5-lipoxygenase Alox5[3,5,6]. LTB_4 acts on its cognate receptor BLT1 to relay chemotactic signals to neighboring neutrophils, thereby broadening their recruitment range to inflamed/injured sites[7,8], where neutrophils engage with the microenvironment, secrete a variety of molecules, and help recruit other immune cells, to promote host defense in a timely manner[1]. When finished with their task, neutrophils die either at the injury site or after migrating back to the bone marrow[8,9].

LTB_4 is considered to be one among several chemoattractants that contribute to neutrophil arrest and extravasation from the vasculature[10]. Studies in mice that do not produce LTB_4 (*Alox5*$^{-/-}$) or lack its receptor (*Blt1*$^{-/-}$) have highlighted the critical role of the LTB_4-BLT1 axis in mobilizing neutrophils and other myeloid cells across the blood vessel in multiple models of injury. However, whether the LTB_4 generated by neutrophils is necessary and sufficient to elicit the cascade of events that leads to their extravasation in response to infection remains to be determined. To this end, we used an *in vivo* model system based on the use of ISMic, which allows the imaging of dynamic biological processes in live animals at subcellular resolution[11,12]. Here, we report (i) a crucial role for neutrophil-derived LTB_4 in regulating the dynamics of the key regulators NMIIA and Itgb2; and (ii) that the LTB_4-mediated autocrine/paracrine signaling pathway, which promotes neutrophil arrest and extravasation responses *in vivo*, is blocked by treatments that inhibit the release of exosomes from the cell.

RESULTS

The LTB_4-BLT1 axis is required for the persistent recruitment, rolling, arrest and extravasation of neutrophils in response to infection

To assess the role of the LTB_4-BLT1 axis during neutrophil extravasation, we developed an *in vivo* inflammation model based on the injection of heat-killed *E. coli* into the hind footpad of anesthetized mice (Figs. 1A and 1B). First, we set up the optimal conditions for imaging neutrophil extravasation in a mouse strain expressing GFP in myeloid cells (*LyzM-GFP*)[13]. Upon infection, neutrophils accumulated in the blood vessels and extravasated (Fig. 1A right panel, pink arrows, and Movie S1), whereas under control conditions, we observed no neutrophil retention in the vasculature (Fig. 1A left panel and Movie S1). Similar results were obtained using an adoptive transfer model, where neutrophils were purified from the bone marrow of a *WT* mouse, labeled with a cell-permeant fluorescent dye and injected into a recipient WT mouse (Fig. 1B, pink arrows and Movie S2). Using the latter approach, we infected the footpad of *Alox5*$^{-/-}$ mice, which are incapable of producing LTB_4, and introduced neutrophils purified from either *WT* or *Alox5*$^{-/-}$ mice (Fig. 1C). We observed that up to 3 hours post-infection, the recruitment of *Alox5*$^{-/-}$ neutrophils to the infected footpad was significantly reduced in comparison to *WT* neutrophils (Figs. 1C & 1D). To gain further insights into this process, we visualized the intravascular dynamics of *WT* and *Alox5*$^{-/-}$ neutrophils introduced into the infected *Alox5*$^{-/-}$ mice (Fig. 1EI & II). Quantitative analysis revealed that ~70% of *WT* neutrophils displayed rolling, ~40% showed arrest in the lumen of the blood vessels, and ~20% extravasated in response to infection (Fig. 1F & Movie S2). Conversely, *Alox5*$^{-/-}$ neutrophils displayed significantly reduced rolling (~20%), arrest (<10%) and extravasation response (<5%) (Figs. 1EII & 1F; Movie S3). A similar defect was observed in *Blt1*$^{-/-}$ neutrophils, which lack the receptor for LTB_4, when introduced in either *Alox5*$^{-/-}$ (Figs. 1EIII & 1F; Movie S4) or *Blt1*$^{-/-}$ mice (Figs. 1EIV & 1F; Movie S4). Collectively, these findings establish that LTB_4 produced by neutrophils signals via the BLT1 receptor to promote neutrophil rolling, arrest, and extravasation response to infection *in vivo*.

The LTB_4-BLT1 axis regulates the polarized redistribution of NMIIA and Itgb2 during neutrophil arrest

A downstream target of LTB_4 signaling in neutrophils stimulated with primary chemoattractant is the actin-based motor NMIIA[7,14]. To determine if NMIIA activation is required for neutrophils extravasation, we inhibited Rho Kinase (ROCK), a key enzyme that controls the activation and assembly of NMIIA filaments by phosphorylating two residues (S19 and T18) on the myosin light chain[15]. We found that pretreatment of *WT* neutrophils with the ROCK inhibitor Y27632[15] significantly reduced their arrest and extravasation response in the infected *Alox5*$^{-/-}$ mouse footpad, when compared to vehicle-treated neutrophils (Figs. 2A & 2B). This finding prompted us to assess whether the LTB_4-BLT1 axis also regulates NMIIA dynamics during neutrophil arrest and extravasation *in vivo*. Neutrophils were purified from a knock-in mouse expressing *GFP-NMIIA*[16] and treated with either the vehicle or MK886, a covalent non-reversible inhibitor of the 5-lipoxygenase adapter protein (FLAP)[17], before being introduced into infected *Alox5*$^{-/-}$ mice. The extent of the arrest and extravasation of the vehicle-treated *GFP-NMIIA* neutrophils was indistinguishable from that of *WT* neutrophils (Figs. 2C left panel & 2D; compare with Fig. 1F). However, treatment with MK886 led to a reduction of both the arrest and extravasation of *GFP-NMIIA* neutrophils (Figs. 2C right panel & 2D), consistent with our observations in *Alox5*$^{-/-}$ neutrophils. Next, we used ISMic to (i) visualize GFP-NMIIA dynamics in neutrophils that displayed arrest within the vasculature, and (ii) score for its cellular distribution. We found that treatment with MK886 significantly prevented the redistribution of NMIIA from the cytoplasm to the cell cortex that we observed in vehicle-treated neutrophils (Figs. 2E, 2F & S1; Movie S5). This finding established that LTB_4 signaling in neutrophils is required for the polarized redistribution of NMIIA *in vivo*. We also attempted to address whether F-actin dynamics are regulated by the LTB_4-signaling axis within neutrophils, using neutrophils derived from a mouse expressing the F-actin probe GFP-Lifeact[18]. Unfortunately, although *GFP-Lifeact* neutrophils exhibited rolling and adhesion along the blood vessels, they were defective in their extravasation response *in vivo*, suggesting a possible inhibitory effect of this probe (not shown). Overall, we conclude that the LTB_4-BLT1 axis promotes the dynamic and polarized redistribution of NMIIA to aid neutrophil arrest and extravasation response to infection.

We next sought to address how NMIIA controls arrest and extravasation in neutrophils. Leukocytes adhesion to blood vessels is regulated by the interaction between

Itgb2 expressed on their plasma membrane (PM) and adhesion molecules expressed on the endothelial surface (e.g., ICAMs). Consistent with this idea, *Itgb2*$^{-/-}$ neutrophils, when introduced in *Alox5*$^{-/-}$ mice, displayed severe defects in arrest and extravasation in response to infection (Figs. 3A & 3B), similar to *Alox5*$^{-/-}$ neutrophils (Figs. 1E & 1F). We therefore hypothesized that the LTB_4-BLT1-myosin pathway regulates the localization and dynamics of Itgb2 at the PM to promote its engagement with the ICAM1/2 on the endothelium. To this end, we incubated purified *WT* and *Alox5*$^{-/-}$ neutrophils with a fluorescently-conjugated antibody directed against Itgb2 (M18/2 clone) and introduced them into infected *Alox5*$^{-/-}$ mice to directly visualize Itgb2 in neutrophils. The antibody bound specifically to Itgb2 (Fig. 3C) and did not impact the extravasation response of labeled *WT* neutrophils *in vivo* (Fig. 3D & Movie S6). In *WT* neutrophils rolling in the blood vessels, Itgb2 localized to dispersed cytoplasmic structures (Fig.3D left panel & Movie S6). As *WT* neutrophil arrested, Itgb2 redistributed to areas of the cell periphery that were in direct contact with the endothelium (Fig. 3D middle panel & Movie S6). Later on, as *WT* neutrophil protruded and extravasated into the interstitium, Itgb2 gradually redistributed to the back of the migrating cell (Fig. 3D right panel & Movie S6). Conversely, in *Alox5*$^{-/-}$ neutrophils that transiently arrested in the blood vessels and did not extravasate, Itgb2 was primarily confined to an intracellular pool and failed to redistribute to the cell periphery (Figs. 3E & 3F; Movie S6). A similar defect in Itgb2 redistribution was observed in *WT* neutrophils that were pre-treated with the ROCK inhibitor Y27632 (Fig. 3F). These findings suggest that NMIIA activation via LTB_4 signaling contributes to the dynamic redistribution and localization of Itgb2 on the neutrophil PM, to facilitate sustained interaction with the ICAMs on the endothelium.

The LTB_4-BLT1 axis promotes adhesion, actomyosin polarization and ITGB2 trafficking in primary human neutrophils

LTB_4 was first identified as a signal-relay molecule in promoting chemotaxis response of primary human neutrophils (PMNs) to primary chemoattractant[7]. Since we identified the LTB_4-BLT1 axis as a key regulator of arrest and extravasation in mouse neutrophils responding to infection, we investigated if such a mechanism operates during PMN adhesion in response to primary chemoattractants. To this end, we plated PMNs on

a fibrinogen-coated surface to promote adhesion response to chemoattractant stimulation. PMNs pre-treated with the vehicle, showed a progressive increase in their ability to adhere upon stimulation with the bacterial peptide analogue fNLFNYK (Fig. 4A). However, pre-treatment with MK886 or LY223982, a BLT1 antagonist[19], significantly reduced adhesion at later time points (Fig. 4A), without affecting the initial adhesion response. Importantly, the requirement of the LTB_4-BLT1 axis for sustained PMN adhesion response was specific to end-target (fNLFNYK and C5a) but not intermediate (CXCL8) chemoattractants (Fig. S2A), consistent with the previously described signal-relay function for the LTB_4-BLT1 axis during chemotactic migration [7,14]. Furthermore, treatment with MK886 or LY223982 reduced cortical NMIIA and polarized F-actin distribution in PMNs (Figs. 4B & 4C). Therefore, the LTB_4-BLT1 axis relays signals to promote actomyosin polarity and sustained adhesion of PMNs in response to primary chemoattractants.

Given the limitations of our IVM-based approach, we used time-lapse confocal imaging to study the dynamics of human Itgb2 (ITGB2) in PMNs. To this end, we used an Alexa 488-conjugated antibody to label ITGB2 (CTB104 clone, hereafter called fluorescent αITGB2) in PMNs. We found that, as the PMN responded to fNLFNYK stimulation by spreading, ITGB2 quickly redistributed from the PM into a ring-like structure at adhesion sites, where PMNs engaged with the substrate (Fig. 4D white arrows & Movie S7A), consistent with the redistribution observed in mice (Fig. 3D). As time progressed and the PMNs began to migrate, we observed the disassembly of the ring-like structure and the formation ITGB2-containing endocytic vesicles at the back of the PMNs (Fig. 4D blue arrowheads & Movie S7A), similar to the behavior of primary chemoattractant GPCRs in activated PMNs[14]. Upon inhibition of LTB_4 signaling by LY223982, we observed a rapid formation and internalization of ITGB2, which failed to assemble into a ring-like structure at the bottom of PMNs (Fig. 4E blue arrowheads & Movie S7B). Additionally, we observed a significant increase in the number of ITGB2-containing vesicles (Figs. S2B & S2C). This finding prompted us to further investigate the regulation of ITGB2 trafficking by the LTB_4-BLT1 axis in PMNs. In polarized vehicle-treated PMNs, we found that ITGB2 clusters largely localized at the PM facing the adhesion site (Fig. 4FI), as revealed by the quenching the fluorescence of the αITGB2 antibody following

incubation with a cell-impermeant antibody directed against the fluorophore (Fig. 4FII). On the other hand, in MK886-treated PMNs most of the αITGB2 fluorescence showed a punctate intracellular distribution, which persisted after treatment with the quenching antibody (Fig. 4FIII & 4FIV). We next investigated the internalization and recycling of ITGB2 in PMNs. First, using inhibitors to specific endocytic pathways, we confirmed that the internalization of αITGB2 occurred via a clathrin-independent and dynamin-dependent endocytic pathway (Figs. S2D & S2E), as previously described[20]. Second, upon treatment with inhibitors of either the LTB_4-BLT1 axis or ROCK, we found that the extent of internalized ITGB2 substantially increased (~3-4 folds), compared to the vehicle (Fig. 4G). Finally, we found that the extent of increase in the internalized ITGB2 corresponded to a block in the recycling of ITGB2 back to the PM, since only ~15% of the internalized ITGB2 was cleared upon inhibition of the LTB_4-BLT1-myosin pathway, compared to 60% in the control (Fig. 4H). Together, these findings show that in human neutrophils, the LTB_4-BLT1-myosin axis promotes recycling of ITGB2 from an intracellular pool as well as its retention on the PM, which is consistent with our observations in living mice.

The autocrine/paracrine action of LTB_4 relies on exosome production

The finding that the LTB_4 produced by neutrophils is necessary for their extravasation *in vivo* prompted us to further investigate whether this process occurs in an autocrine/paracrine fashion. To this end, we assessed whether the defect in arrest and extravasation behavior observed in *Alox5*$^{-/-}$ neutrophils could be rescued by co-injection of *WT* neutrophils, which produce LTB_4 (Fig. S2F). Under these conditions, we found that *Alox5*$^{-/-}$ neutrophils displayed robust rolling, arrest, and extravasation comparable to *WT* neutrophils (Figs. 5AI & 5B; Movie S8). Importantly, blocking LTB_4 production in *WT* neutrophils using MK886 impaired the ability of WT neutrophils to rescue the *Alox5*$^{-/-}$ defect in rolling, arrest and extravasation (Figs. 5AII & 5B; Movie S8). We next sought to investigate whether LTB_4 is packaged and released via exosomes, as described in neutrophils during LTB_4-mediated chemotactic signal-relay *in vitro* [21]. Specifically, we investigated whether the small GTPase Rab27a and neutral sphingomyelinase (N-SMase) that were reported to regulate the release of exosomes from neutrophils[21],

contributed to their extravasation response *in vivo*. We found that treatment of *WT* neutrophils with the Rab27a inhibitor Nexinhib20[22], prevented the arrest and extravasation, of both WT and *Alox5*$^{-/-}$ neutrophils in the co-injection model (Figs. 5AIII & 5B; Movie S8). A similar effect, was observed upon treatment with the N-SMase inhibitor GW4869[23], which is also known to block exosome formation, but not the control drug Exo1[24] (Figs. 5AIV-V & 5B; Movie S8). Importantly, treatment with Nexinhib20 impaired the redistribution of Itgb2 *in vivo* (Fig. 5C), phenocopying our observation in *Alox5*$^{-/-}$ and *WT* neutrophils treated with Y27632 (Fig. 3F), and suggesting that the Rab27a-mediated exosome release is required for LTB_4 to relay signals effectively. Additionally, treatment of PMNs with Nexinhib20 or GW4869 (but not Exo1) resulted in impaired actomyosin polarization, enhanced ITGB2 internalization, and reduced adhesion response *in vitro* (Figs. 5D-G). Together, these findings suggest that exosomes facilitate the relay of LTB_4 in an autocrine/paracrine manner to promote neutrophil arrest and extravasation response to infection (Fig. 5H).

DISCUSSION

Neutrophils respond to inflammation by sensing a combination of chemoattractants and chemokines, which elicit a sequence of events in the vasculature that includes: engagement with ligands on the endothelial cells, adhesion, and extravasation[10,25,26]. How chemoattractants production and action is spatio-temporally controlled *in vivo* has only begun to be appreciated, as revealed by recent reports in select mouse models [27–29]. In the present study, we used intravital microscopy in live mice, combined with specific *in vitro* assays involving PMNs, to investigate and unravel the specific role of the LTB_4/BLT1 axis in controlling intravascular neutrophil dynamics in response to sterile bacterial infection. Using pharmacological and genetic tools, we found that a block in either LTB_4 production or its receptor BLT1 inhibits neutrophil arrest and extravasation and co-adoptive transfer experiments revealed that LTB_4 operates in an autocrine and/ or paracrine fashion. Importantly, inhibitors to the small GTPase Rab27a and N-SMase, which have been shown to regulate the release of LTB_4-containing exosomes in neutrophils *in vitro*[21], also reduced neutrophil rolling, arrest, and extravasation behavior in our co-adoptive transfer model, phenocopying the effects of the LTB_4 inhibitor and underscoring the role for exosomes in amplifying the early neutrophil intravascular response to infection. We envision a scenario in which neutrophils release exosomes into the vasculature, in proximity to the site of inflammation. Based on the finding that exosomes have been found to harbor ITGB2 during inflammation[30], we speculate that they would tether to the endothelium in an ITGB2-dependent fashion, and locally produce and release LTB_4. LTB_4 is then sensed in either an autocrine or paracrine fashion through the BLT1 receptor to promote sustained arrest and extravasation response (summarized in Fig. S3). Overall, our findings could bear important clinical relevance, as LTB_4 production and exosome generation in neutrophils are intimately associated with the progression of diseases including tumor metastasis[31] and chronic inflammatory lung disorder[30] respectively.

Since LTB_4 regulates neutrophil adhesion both *in vivo* and *in vitro*, we focused on the possible downstream targets, and among them NMIIA, the only member of the NMII family of actin-based motors expressed in neutrophils. During their response to inflammatory stimuli, neutrophils display a striking LTB_4-dependent redistribution of

NMIIA both *in vivo* and *in vitro*. Specifically, in rolling neutrophils, NMIIA is primarily restricted to the cytoplasm. As neutrophils arrest and prepare to extravasate, NMIIA rapidly redistributes to the cortex at the back of cells, posing the question as to how NMIIA is implicated in neutrophil extravasation. One possibility is that, as shown in migrating neutrophils *in vitro*, ROCK-mediated NMIIA contractile activity is required to retract the rear of the cell in coordination with the protrusive activity of the front, that is primarily controlled by dynamic F-actin formation[32]. Consistent with this model, we observed F-actin accumulation at the protrusive front in PMNs *in vitro*, and NMIIA distribution to the back of murine neutrophils *in vivo* and PMNs *in vitro*. Therefore, NMIIA likely provides the contractile force required for neutrophils to squeeze through extravasation sites after arrest. However, our finding that NMIIA activity contributes to neutrophil arrest *in vivo*, prompted us to investigate its possible role in adhesion. Indeed, it has been proposed that NMIIA can regulate integrin-based adhesion stability during cell migration via different non-exclusive mechanisms[33]. In live mice, we demonstrated that neutrophil adhesion requires the key integrin Itgb2, which is consistent with its proposed role during neutrophil arrest[32,43]. Importantly, we showed its dynamic redistribution from a dispersed intracellular pool to a defined area of the neutrophil surface that is juxtaposed to the endothelial wall of blood vessels, consistent with the observed distribution of LFA-1 in neutrophils transmigrating through endothelial cell layers *in vitro*[35].

Although ISMic is a powerful approach that we have used in the past to track endocytic events in other systems [36,37], due to the depth of the field of view in the mouse footpad, we could not image the fate of the Itg2-containing intracellular structures with sufficient temporal and spatial resolution. However, complementary work using PMNs *in vitro*, which recapitulate most of the features of neutrophils adhesion and crawling, indicates that initially ITGB2 is rapidly redistributed from the PM to the adhesion site, where it forms an adhesion ring, that, as PMNs begin to migrate, is disassembled using a process that involves ITGB2 internalization (Fig. S3). In the initial step of adhesion, we could not resolve whether, ITGB2 clusters at adhesion sites through lateral diffusion or if it is rapidly internalized and recycled back to the PM at the bottom of the cells. We favor the latter explanation since inhibition of the LTB_4-BLT1 axis resulted in: (i) a block in the formation of the ITGB2 adhesion structure; (ii) an increase in ITGB2 internalization; and

(iii) in the inhibition of ITGB2 recycling to the PM (Fig. S3). Notably, these defects were phenocopied upon inhibition of NMIIA activation, thus strongly indicating a link between ITGB2 trafficking and NMIIA. Whether NMIIA activation directly promotes ITGB2 recycling or negatively regulates its internalization has yet to be determined. Interestingly, during T cell migration NMIIA and ITGB2 have been shown to directly interact to promote de-adhesion[38]. However, NMIIA regulation of ITGB2 *in vivo* is likely to be indirect, since they are localized, respectively, to the rear and the front of arrested and extravasating neutrophils. Since NMIIA activity has been shown to be required for the maintenance of lipid microdomains on the neutrophil PM[39], it is conceivable that NMIIA, at the rear of the cells, creates domains that limits ITGB2 internalization and recycling. This would force ITGB2 to internalize and rapidly recycle at the actin-rich front of the cells, thus confining its localization to adhesion sites. As the cells begin to extravasate and resume migration, the adhesion structures are disassembled by enhancing ITGB2 internalization. On the other hand, in the absence of the LTB_4-BLT1 signal, NMIIA and F-actin controlled microdomains may not form, thus resulting in enhanced internalization and inhibition of overall ITGB2 recycling, possibly by diverting its trafficking to a slow recycling pathway. The net result would be a reduction in ITGB2 levels at adhesion sites, leading to an impairment in stable arrest and, consequently, in neutrophil extravasation. Similar defects have been documented for LFA-1 and α3ß1 integrins, respectively, under different contexts[40,41].

Overall this study demonstrates a novel role for the LTB_4-BLT1 signaling axis in neutrophil extravasation, which complements its already established role as a signal relay axis during neutrophil interstitial chemotaxis[7,8]. Our combined *in vivo* and *in vitro* approaches provide a platform to dissect complex intracellular steps, involving the coordination of membrane trafficking events (ITGB2 recycling) and signaling (LTB_4-BLT1 axis) with that of actomyosin dynamics, which together orchestrate the dynamics of neutrophil activities such as adhesion, extravasation and interstitial migration, that are fundamental to innate immune cell response.

ACKNOWLEDGEMENTS

This research was supported by the Intramural Research Program of the National Institutes of Health, National Cancer Institute and Center for Cancer Research. We thank Drs. Dorian McGavern (NINDS) and Robert S. Adelstein (NHLBI), for providing us the *LyzM-GFP* and *GFP-NMIIA* mouse lines respectively. We thank the animal facilities of NCI and Dr. Wang-Ting Hsieh, FNLCR, for maintaining and genotyping the animals respectively. We also thank Dr. Michael Kruhlak and Langston Lim, CCR confocal core, for their help with confocal microscopy.

AUTHOR CONTRIBUTIONS

Conceptualization - B.C.S, R.W and C.A.P; Methodology – B.C.S, N.M, W.W R.W. and C.A.P.; Investigation – B.C.S, N.M, D.C and D.G; Analysis – B.C.S and D.C; Writing, original draft – B.C.S, R.W and C.A.P;

DECLARATION OF INTERESTS

The authors declare no competing interests.

MATERIALS AND METHODS

Mice

The following strains: *C57BL/6J (WT)*, *Alox5*$^{-/-}$ (B6.129S2-*Alox5*^{tm1Fun}*/J*), *Blt1*$^{-/-}$ (B6.129S4-*Ltb4r1*^{tm1Adl}*/J*) and *Itgb2*$^{-/-}$ (B6.129S7-*Itgb2*^{tm1Bay}*/J*) were obtained from JAX (The Jackson Laboratory, Bar Harbor). *LyzM-GFP*, *GFP-NMIIA* and *GFP-Lifeact* mice were obtained from Drs. Dorian McGavern (NINDS, NIH), Robert Adelstein (NHLBI, NIH) and from Roland Wedlich-Söldner[18], respectively. The study was approved and conducted in accordance with the animal protocols approved by the Institutional Animal Care and Use Committee, protocols – LCMB-031 and LCMB-035 (National Cancer Institute). Mice, both males and females, were used for the experiments at an age between 2-6 months.

Reagents

Antibodies against mouse Itgb2 (clone M18/2; Alexa Fluor 594 conjugated), NMIIA heavy chain (Poly19098) and custom Rhodamine-conjugated antibody to CD31 (clone 390) were from BioLegend, Inc. Antibodies against CD31 (clone 390; eFluor450 conjugated) and for quenching Alexa Fluor 488 were from Invitrogen. Antibodies against CD16/32 (Fc block; clone 2.4G2) and ITGB2 (clone CTB104; Alexa Fluor 488 conjugated) were from BD Pharmingen and Santa Cruz Biotechnology Inc., respectively. *E. coli* bioparticles (K12-strain; Texas red conjugated), CellTracker Green CMFDA, CellTracker Red CMPTX, CellMask Deep Red for PM and Rhodamine Phalloidin dyes were from Molecular Probes. PitStop2, MDC and fibrinogen (human plasma derived) were from Sigma Aldrich. Recombinant fNLFNYK, human C5a and human CXCL8 were from Santa Cruz Biotechnology Inc., R&D systems and Peprotech Inc., respectively. LTB_4, LY223982, Y27632 and GW4869 were from Cayman Chemical. MK886, Nexinhib20, Exo1, Dynasore and MitMAB were from Tocris Bioscience.

Primary neutrophil isolation from mice and human samples

Mouse neutrophils were obtained from the bone marrows of front and hind limbs. Briefly, cells were flushed out using RPMI without phenol red medium (Invitrogen) supplemented with 1 mM HEPES (Gibco) and antibiotics (Gibco) (hereafter called RPMI medium) and

filtered via a 40 µm cell strainer (Corning Inc.). Subsequently, red blood cells were lysed using ACK buffer (Gibco) for 30 secs, layered onto a discontinuous gradient of Histopaque 1077 (Sigma Aldrich) and Histopaque 1119 (Sigma Aldrich), in a 1:1:1 ratio as previously reported[42]. Neutrophils were isolated from the 1077/1119 Histopaques interface, rinsed and resuspended in RPMI medium. Human neutrophils (PMNs) were obtained from heparinized whole blood of healthy human donors by venipuncture, as part of the NIH Blood Bank research program and purified as reported previously [14]. Red blood cells were lysed by multiple rounds of exposure to hypotonic solutions (0.2% NaCl in water; 30 secs) followed by the addition of a neutralizing solution (1.6% NaCl in water), and then centrifugation. Isolated primary neutrophils were resuspended in RPMI medium and incubated on a rotator at room temperature (hereafter called RT) for further experimentation. All the inhibitor treatments and chemoattractant stimulation experiments *in vitro* were performed at 37° C.

Adoptive transfers and infection model

Mouse neutrophils (~10^7 cells) isolated from WT mice were labeled with either the cytosolic dye CellTracker Green CMFDA or CellTracker Red CMPTX, whereas neutrophils isolated from mice expressing GFP-NMMIA or GFP-Lifeact were left unstained. In selected experiments, neutrophils were treated with inhibitors of LTB_4 production (MK886), ROCK activity (Y27632), Rab27a (Nexinhib20), N-SMase (GW4869), ER-golgi transfer (Exo1) or DMSO (0.2 % in volume) as vehicle control for 20 mins in RT. For Itgb2 visualization *in vivo*, DMSO- or inhibitor-treated neutrophils were incubated for 10 mins with Fc-block antibody (2.5 µg per ~10^7 cells), followed by 10 mins incubation with anti-Itgb2 antibody (M18/2 clone) conjugated to Alexa 594 (5 µg per ~10^7 cells), washed and adoptively transferred into the mice. Stained neutrophils (~6-8 x 10^6) resuspended in saline were co-injected with antibody to CD31 (clone 390; 15 µg) conjugated to either Rhodamine or eFluor450 dye through tail vein injection. For co-adaptive transfer experiments, neutrophils purified (~6-8 x 10^6 each) from *WT* mouse and *Alox5*$^{-/-}$ were labeled with different dyes, mixed in 1:1 ratio, and adoptively transferred. The recipient mice were anesthetized by an intraperitoneal injection of a mixture of 100 mg/Kg ketamine (VET One) and 20 mg/Kg xylazine (Anased LA; VET One). ~3-5 x 10^3

heat killed *E. coli* (~10-15 µl) were gently injected into the hind footpad, using a syringe equipped with a 33 G needle (TSK Laboratory), without damaging the blood vessels and the tissue. In experiments involving inhibitors or ISMic, the recipient mice underwent short-term anesthesia by isoflurane inhalation (Forane; Baxter Healthcare Corp.), infected with *E. coli* in the footpad and allowed to recover for 45 mins prior to the adoptive transfer of neutrophils along with the conjugated anti-CD31 antibody. In the case of *LyzM-GFP* mice, the anti-CD31 antibody was injected *IV* prior to anesthesia. One footpad was injected with saline as control, whereas the other was injected ~1 h after with *E. coli.*

IVM and ISMic of the infected footpad

The infected footpad of anesthetized mouse was placed in a custom-designed holder to ensure stability, with the entire stage heated and maintained at 37° C during the entire imaging period. Imaging was performed by using an inverted laser-scanning two-photon microscope (MPE-RS, Olympus, Center Valley, PA, USA) equipped with a tunable laser (Insight DS+, Spectra Physics, Santa Clara, CA, USA). Excitation was performed at 850 nm for the experiments with GFP-NMIIA neutrophils and 810 nm for all the other experiments. Emitted light was collected by an appropriate set of mirrors and filters on 3 GaAs detectors (bandpass filters: Blue = 410–460 nm, Green = 495–540 nm, Red = 575–645 nm). Images were acquired using a 37°C heated objective: 10X air objective (NA 0.4), 30X and 40X silicone oil immersion objectives (NA 1.05 and 1.25 respectively, UPLSAPO, Olympus). Imaging was performed by continuous acquisition of 20-25 Z-stacks (3 µm step size and at a frame rate of ~6-10 secs between frames) for a total period of 15-20 minutes for individual field of view (hereafter called FOV). For ISMic, we used both 30x and 40x objectives, with a digital zoom of 3-4x, acquiring 8-10 Z-stacks with 2 µm step size and at a frame rate of ~6-8 secs between frames for a total period of 5-10 minutes for individual FOV. Images were acquired using the Olympus Fluoview software and processed for further analysis using Fiji, Imaris (Bitplane) and MATLAB (Math Works).

Analysis of neutrophil recruitment kinetics in the infected footpad

The Z-stacks shown in Figures 1B and 1C were acquired by IVM using a 10X air objective at fixed time points after the infection. Maximal projections of the stacks were used to quantify the neutrophils in each FOV using the Imaris spot detection function at each time point. A single FOV using the 10X air objective was sufficient to capture a large area with extravasation event, which was followed over multiple time points. The numbers of neutrophils were normalized and represented as fold change with respect to 1 h post infection. The number of neutrophils observed at 1 h post infection observed in the footpad between adoptively transferred *WT* or *Alox5*$^{-/-}$ neutrophils was comparable across experiments.

Analysis of intravascular neutrophil behavior

First, we corrected for the motion artifacts due to heartbeat and respiration by applying to the raw time-lapse images a customized MATLAB function based on max cross-correlation image registration algorithm[43]. Next, we determined the outline of the blood vessels for each time frame by segmentation of the maximal projections derived from the volume rendering of the aquired Z-stacks. Neutrophils contours were identified using a snake algorithm implemented with MATLAB scripts, as previously described [44,45], and they were overlaid to the max intensity projection of the blood vessels. To measure neutrophil velocity we used a manual tracking plugin in Fiji. To determine their position with respect to the blood vessels we calculated the overlap fraction (OF). For each cell at each frame, the OF was calculated as the area of the 2-D max projection of the cell overlapping with the segmented blood vessels divided by the total cell area. Neutrophils were considered inside the blood vessels if the OF exceeded 0.5. Neutrophils were classified as showing free-flowing, rolling, arrest or extravasation behavior according to the following criteria: 1) free-flowing, if the velocity was higher than 1 μm/s and the OF > 0.5; 2) rolling, if the velocity was between 0.15 and 0.5 μm/s and the OF > 0.5; 3) arrest, if the velocity was lower than 0.15 μm/s and the OF > 0.5; and 4) extravasation, if the OF dropped below <0.5. The neutrophil behavior were scored and represented independently for each cell in the field of view (FOV). As a neutrophil can show one or more behavior during the course of acquisition, it is scored for each behavior independent of the other

and therefore the % cells that display rolling, arrest and extravasation will not add up to 100% by this analysis. Multiple FOVs were imaged in each experiment and typically data sets between 1-2 h post infection were considered for analysis, with the data normalized and presented as % cells across FOVs that exhibited rolling, arrest and extravasation for each experiment in each condition. For the experiments involving Y27632 and MK886 treatments in Figs. 2A and 2B, the % of cells that arrested and extravasated were scored manually from multiple FOVs in each ISMic imaging experiment.

Analysis of NMIIA and Itgb2 peripheral distribution index

We acquired Z-stacks (typically 8-12 stacks) at a frame rate of ~5-8 secs. Only neutrophils that displayed arrest behavior were considered for the time periods - 0, 30, 60 and 90 secs of arrest within the blood vessel. In every frame, we identified the sections corresponding to a give cell and determined the cortical redistribution of either GFP-NMIIA or Itgb2 by assigning a value of 0 for a centrally distributed fluorescent signal within the cell, and 1 for a cortically distributed fluorescent signal at the cell periphery. For each cell, we averaged the scores determined in each section of the stack to the total number of stacks analyzed and the index for each cell analyzed is presented.

In vitro adhesion assay and the analysis of actomyosin polarity

Neutrophils (2 x 10^5 cells) were plated in 8-well chambers with a bottom coverglass coated with 100 µg/ml of fibrinogen (Lab-Tek; #1 NA). All the experiments were performed at 37˚ C. Cells were pretreated with vehicle (DMSO; 0.2% in volume) or specified inhibitors for 20 mins before stimulation with chemoattractants. Post stimulation, cells were gently washed with RPMI, fixed with 4% PFA and stained with DAPI (10 ng/ml) and rhodamine phalloidin (0.2 Units). For the analysis of cortical distribution of NMIIA, cells were permeabilized with a buffer (0.5% Saponin and 0.5% Triton X 100, both from Sigma Aldrich) for 5 mins at 37˚ C, followed by staining with anti-NMIIA antibody (in 1% FBS containing PBS) overnight at 4˚ C and thereafter with a secondary antibody for 2 h in RT. Images were acquired by using an 880 Airyscan microscope equipped with the ZEN software (Carl Zeiss) using either 20X (Zeiss Plan Apochromat 20X/ 0.8 air) or 40X (Zeiss Plan Apochromat 40X/ 1.4 oil) lenses. The number of cells per FOV were estimated by

measuring the DAPI signal using the Imaris spot detection method. Typically, more than a hundred cells per condition were analyzed from multiple FOVs. For the kinetic analysis of adhesion response reported in Figure 4A, the number cells from FOVs were averaged for each time point and represented as fold change with respect to unstimulated controls. For the other experiments, results were normalized and represented as % of the vehicle treated controls. Rhodamine phalloidin and NMIIA staining was used to manually quantify the % cells in each FOV exhibiting polarized F-actin and cortical NMIIA distribution and averaged for each condition in an experiment. Typically, around 100 cells or more per condition were analyzed from multiple FOVs in each experiment to determine actomyosin polarity in PMNs.

Analysis of ITGB2 vesicle trafficking in vitro

For live cell imaging, Alexa 488-conjugated anti-ITGB2 antibody (αITGB2, CTB104 clone, 2 µg) and CellMask deep red (100 nM) were added to vehicle- or inhibitor-treated PMNs plated on fibrinogen-coated surface, before stimulation with 100 nM fNLFNYK and thereafter imaging for ~10 mins post-stimulation. Images were acquired in time-lapse by using an 880 Airyscan microscope using the 63X (Zeiss Plan Apochromat 63X/ 1.4 oil) lens. For the analysis of ITGB2 internalization, Alexa Fluor 488 conjugated αITGB2 (0.1 µg/ml) was added to vehicle or inhibitor pre-treated PMNs, before stimulating with fNLFNYK. After 10 min, cells were fixed and incubated overnight at 4˚C with an anti-Alexa488 functional antibody (0.5 µg per well) to quench the αITGB2 signals on the PM. Samples were counter-stained with DAPI and Phalloidin. Internalized ITGB2 was detected using either epifluorescence (Revolve FL, FJSD1000 from ECHO Laboratory) or confocal (Carl Zeiss 880 Airyscan microscope & ZEN software) microscopes equipped with 40X or 63X objectives. The number of internalized fluorescent vesicles were determined using the Imaris spot detection method. Typically, more than a hundred cells per condition were analyzed from multiple FOVs. Results were normalized and represented as % or fold change with respect to the fluorescent vesicles detected in the control or vehicle condition. For the ITGB2 recycling experiments, vehicle- or inhibitor-treated PMNs were stimulated in the presence of Alexa Flour 488 conjugated anti-ITGB2 antibody for 15 mins. Cells were gently washed with RPMI and either fixed or incubated

for an additional 45 min in RPMI containing fNLFNYK (with or without inhibitor) to allow ITGB2 recycling. Cells were then fixed and the αITGB2 signals on the PM quenched as described above. The number of internalized fluorescent vesicles were determined using the Imaris spot detection method as described above. Results are presented as the % difference in the detected fluorescent vesicles to that of 15 mins time point.

Quantification and Statistical analysis

Microsoft Excel was used for calculations, the results were plotted and analyzed using Prism (GraphPad Software, Inc.). Statistical tests for each graph and the size of the samples are described in the respective figure legend. In the graphs, *p* value less than 0.05, 0.01, 0.001 and 0.0001 are represented with *, **, *** and **** respectively.

Figure legends

Figure 1. Production and sensing of LTB_4 via BLT1 in neutrophils promote recruitment, rolling, arrest and extravasation during infection.

A-B Set up of the mouse infection model (A) Upper Panel – Diagram of the IVM procedures in the *LyzM-GFP* mouse footpad. Lower panels – Mice were injected with either saline (control, left panel) or *E. coli* (right panel), and the foot pad was imaged after 1 h by IVM. Maximum projections of Z-stacks. Vasculature (blue) and neutrophils (green). Pink arrowheads mark extravasating neutrophils (right panel). See Movie S1. Scale bar 40 µm. The experiments were performed in N=2 mice.

(B) Upper Panel – Diagram of the IVM procedures in a mouse footpad infection and adoptive transfer model. Lower panels - Neutrophils purified from a *WT* background were labeled with CellTracker Green CMFDA adoptively transferred in recipient *WT* mice that were injected with either saline (left panel) or *E. coli* (right panel) and imaged by IVM. - Maximum projections of Z-stacks. Vasculature (blue) and *WT* neutrophils (green). Pink arrowheads mark extravasating neutrophils (right panel). See Movie S2. Scale bar 50 µm. The experiments were performed in N=2 mice.

(C-D) Neutrophil response in the *Alox5*$^{-/-}$ mouse footpad. Neutrophils purified from either *WT* (upper panels) or *Alox5*$^{-/-}$ (lower panels) mice were labeled with CellTracker Green CMFDA and adoptively transferred to *E. coli*-infected *Alox5*$^{-/-}$ mice. **C**- Maximum projections of Z-stacks of the footpads were acquired 1 h, 2 h and 3 h post infection. Scale bar equals 100 µm. **D**- The number of neutrophils recruited to the footpad were scored as described in the Methods section and expressed as fold change with respect to the number of neutrophils scored 1h post-infection. Data are Means ± SEM with N=3 mice per condition. Statistical significance was assessed by a Two-way ANOVA analysis using Sidak's multiple comparisons.

(E-F) Analysis of neutrophil rolling, arrest and extravasation in *Alox5*$^{-/-}$ *and* *Blt1*$^{-/-}$ mice. Neutrophils purified from *WT* (I) or *Alox5*$^{-/-}$ (II) or *Blt1*$^{-/-}$ (III and IV) mice were labeled with CellTracker Green CMFDA and adoptively transferred to *E. coli*-infected *Alox5*$^{-/-}$ (I - III) or *Blt1*$^{-/-}$ (IV) mice. **E**- IVM time-lapse were acquired 1.5h post-infection (see Movies S3 and S4). Still images represent maximum intensity projections of Z-stacks. Neutrophils (green)

and blood vessels (blue). The dashed tangerine lines indicate vessel boundaries and magenta arrowheads point to extravasating neutrophils. Scale bar 50 µm. **F**- Neutrophils were scored, as described in the Methods section, for their rolling, arrest and extravasation. Data are expressed as % of neutrophils exhibiting a specific phenotype and represented as Means ± SEM. For each condition the number of animals used were: *WT* Neu in *Alox5*$^{-/-}$ host (N=4), *Alox5*$^{-/-}$ Neu in *Alox5*$^{-/-}$ host (N=3), *Blt1*$^{-/-}$ Neu in *Alox5*$^{-/-}$ host (N=3) and *BLT1*$^{-/-}$ Neu in *BLT1*$^{-/-}$ host (N=4). Statistical significance was assessed through one-way ANOVA analysis using Dunnett's multiple comparison test.

Figure 2. Cortical redistribution of NMIIA during neutrophil arrest requires the LTB_4-BLT1 signaling axis.

(A-B) Neutrophils purified from WT mice were stained with CellTracker Green CMFDA, treated with either 40 µM Y27632 or the vehicle (DMSO) for 20 mins, adoptively transferred into infected *Alox5*$^{-/-}$ mice and imaged by IVM. **A**- Maximum intensity projections of Z-stacks. Magenta arrowheads highlight neutrophils (green) extravasating from the blood vessels (blue). Scale bars 20 µm. **B**- Quantification of the % of neutrophils that exhibited arrest (left panel) or extravasation (right panel). Data is presented as Means ± SEM from N=3 mice for each condition. Unpaired *t* test with Welch's correction was used to determine statistical significance.

(C-D) Neutrophils purified from *GFP-NMIIA* mice were treated with either 5 µM MK886 or the vehicle (DMSO), adoptively transferred into infected *Alox5*$^{-/-}$ mice, and imaged by IVM. **C**- Maximum intensity projections of Z-stacks. Magenta arrowheads highlight extravasating *GFP-NMIIA* neutrophils (green) from the blood vessels (blue). Scale bar equals 20 µm. **D**- Quantification of the % of neutrophils that exhibited arrest (left panel) or extravasation (right panel). Data is presented as Means ± SEM, N=4 mice for vehicle and N=3 mice for the MK886 treatment. Unpaired *t* test with Welch's correction was used to determine statistical significance.

(E-F) Neutrophils purified from *GFP-NMIIA* mice were treated with either the vehicle (DMSO) or 5 µM MK886, injected in infected *Alox5*$^{-/-}$ mice, and imaged in time-lapse modality by ISMic. **E**- Still images represent an individual optical slice from a Z-stack acquired in time-lapse (Movie S5). GFP-NMIIA (white) and blood vessels (blue). Green

arrowhead points to the protrusive front of the extravasating neutrophil. Orange arrowheads indicates a region of cortical NMIIA enrichment. Time is represented in mins:secs. Scale bar 5 µm. **F**– The cortical redistribution of NMIIA was determined as described in the Methods section and in Fig. S1A and represented as redistribution index. Data were collected from 70 cells in N=4 mice and 51 cells from N=3 mice for the vehicle MK886 treatment, respectively. Unpaired *t* test with Welch's correction was used to determine statistical significance.

Figure 3. LTB_4-BLT1 axis regulates Itgb2 dynamics in neutrophils *in vivo*.

(A-B) Neutrophils purified from *Itgb2*$^{-/-}$ mice were labeled with CellTracker Green CMFDA, adoptively transferred into infected *Alox5*$^{-/-}$ mice and imaged by IVM. **A**- Maximum intensity projection of a Z-stack. Dashed tangerine lines indicate vessel boundaries. Scale bar 50 µm. **B** – Quantitative analysis of the % of neutrophils that exhibit rolling, arrest and extravasation. Data is presented as Means ± SEM from N=3 mice.

(C) Neutrophils purified form either *WT* or *Itgb2*$^{-/-}$ mice were labeled with CellTracker Green CMFDA and a fluorescently-conjugated antibody against mouse Itgb2 (M18/2 clone, red), adoptively transferred into infected *Alox5*$^{-/-}$ mice and imaged by ISMic. Maximum intensity projections of Z-stacks are presented. Magenta arrowheads indicate neutrophils positive for Itgb2 staining. The results represent N=3 mice per condition. Scale bar 3 µm.

(D-F) Neutrophils purified form either *WT* or *Alox5*$^{-/-}$ mice were labeled with CellTracker Green CMPTX and fluorescently-conjugated M18/2 antibody (red), adoptively transferred into infected *Alox5*$^{-/-}$ mice and imaged by ISMic. Additionally, *WT* neutrophils were pre-treated with either vehicle (DMSO; D and F) or 20 µM Y27632 (F) and transferred into the recipient. Still images represent maximum intensity projections in xy (large panels) and zy (side panels) derived from time-lapse sequences in Movie S6 (mins:secs), for *WT* neutrophils (**D**) and *Alox5*$^{-/-}$ neutrophils (**E**). CellTracker (Magenta), blood vessels (blue) and Itgb2 (white). Orange and green arrowheads indicate the back and protrusive front of arrested and extravasating neutrophil. Scale bar 5 µm. **F**– The Itgb2 redistribution index was measured as described in the Methods section and presented as individual cells for *WT* (DMSO treated; 70 cells), *Alox5*$^{-/-}$ (59 cells) and *WT* + Y27632 (47 cells) treatments

from N=3 mice per condition. Unpaired *t* test with Welch's correction was used to determine statistical significance.

Figure 4. Human PMNs require LTB_4-BLT1 axis for efficient polarization, ITGB2 trafficking and sustained adhesion response *in vitro*.

(A) PMNs were pre-treated for 20 mins with vehicle or 2 μM MK886 or 20 μM LY223982 and stimulated with 25 nM fNLFNYK on a fibrinogen-coated surface. Cells were either unstimulated (30 mins) or stimulated for 30, 15 and 5 mins prior to fixation. Adhesion was calculated as described in the Methods section and presented as fold change of adhered neutrophils in comparison to untreated controls. Data is represented as Means ± SEM from N=3 independent experiments. Two-way ANOVA analysis using Dunnette's multiple comparison test was used to determine statistical significance.

(B-C) PMNs were pre-treated with the vehicle or 2 μM MK886 or 20 μM LY223982 for 20 mins, stimulated with 25 nM fNLFNYK for 15 mins, fixed and stained with rhodamine phalloidin (magenta) and anti-NMIIA (green). **C**- Representative confocal images for vehicle and LY223982 treated PMNs. Blue and orange arrowheads indicate the front and back of PMNs with polarized actomyosin distribution. Dashed white box indicates the region zoomed and presented on the right side with individual channels in gray scale. Scale bar 5 μm. **C**- Quantification of the % neutrophils exhibiting polarized F-actin and cortical NMIIA in response to above mentioned treatments. Data is represented as Means ± SEM from N=3 independent experiments. One-way ANOVA analysis using Dunnette's multiple comparison test was used to determine statistical significance.

(D-E) PMNs were pre-treated with either the vehicle (D) or 20 μM LY223982 (E) for 20 mins. They were incubated with an Alexa488 fluorescently-conjugated antibody against human ITGB2 (αITGB2, CTB104 clone; white) in combination with CellMask Deep Red (magenta) for ~ 1 min before stimulation with 100 nM fNLFNYK for 10 mins on a fibrinogen-coated surface and acquired as time-lapse 3D imaging using confocal microscopy. See Movie S7. Left panel represents the 3D view of the cell as a function of time (mins:secs). Middle and right panels represent the middle and bottom sections, as indicated by the dashed lines in the 3D view. White arrows indicate the formation of ITGB2

ring-like structure. Blue arrowheads indicate ITGB2 vesicles. Images are representative of 3 independent experiments (see Figs. S2B and S2C).

(F) PMNs were labeled with CellMask Deep Red to visualize the PM (magenta) and with αITGB2 (green), pre-treated with either the vehicle or 2 μM MK886 for 20 mins and stimulated with 25 nM fNLFNYK on a fibrinogen-coated surface. Neutrophils were fixed, and either left untreated (-quenching; I and III) or treated with an anti-Alexa Fluor 488 antibody (+quenching; II and IV). Images represent the maximum intensity projections in xy (large panels on the left) and yz or xz (small panels on the right) dimensions for each condition. The white boxes represent the inset shown in the xz panels. Blue and orange arrowheads indicate surface and internalized anti-ITGB2 signals, respectively. Scale equals 3 μm. Images are representative of N=3 independent experiments.

(G-H) Internalization and recycling of ITGB2**. G**- PMNs were treated with the vehicle or 2 μM MK886 or 20 μM LY223982 or 20 μM Y27632, for 20 min and stimulated with 25 nM fNLFNYK for 10 min on a fibrinogen-coated surface in the presence of αITGB2. Samples were processed and imaged as described in the Methods section to determine the % of the internalized ITGB2. Data are presented as Means ± SEM from N=4 independent experiments. **H**- PMNs were treated with the vehicle or 2 μM MK886 or 20 μM LY223982 or 20 μM Y27632, for 20 min and stimulated with 25 nM fNLFNYK for 15 min on a fibrinogen-coated surface in the presence of αITGB2. Samples were washed and either fixed or stimulated for additional 45 mins in the presence of fNLFNYK and inhibitors, before fixation. Samples were processed and imaged as described in the Methods section to determine the extent of ITGB2 internalization and recycling. Data are presented as Means ± SEM from N=3 independent experiments. One-way ANOVA analysis using Dunnette's multiple comparison test was used to determine statistical significance.

Figure 5. Extracellular vesicles mediate the autocrine/paracrine action of LTB_4 during neutrophil arrest and extravasation response.

(A-B) WT neutrophils labeled with CellTracker Green CMFDA, were pre-treated with vehicle (DMSO; I) or 5 μM MK886 (II), 2 μM Nexinhib20 (III), 20 μM GW4689 (IV) or 40 μM Exo1 (V), and co-injected into infected *Alox5*$^{-/-}$ mice with *Alox5*$^{-/-}$ neutrophils labeled with CellTracker Red CMPTX . **A**- Maximum projections of Z-stacks acquired by IVM. See

Movie S8. Blood vessels are in blue and dashed orange lines indicate vessel boundaries. Orange arrowheads point to extravasated neutrophils. Scale equals 40 μm. **B -** Analysis of % of neutrophils displaying rolling, arrest and extravasation in the above-mentioned conditions. Data is presented as Means ± SEM from N=3 mice per group. Two-way ANOVA analysis using Dunnett's multiple comparison test was used to determine statistical significance.

(C) *WT* neutrophils were labeled with CellTracker Green CMFDA and fluorescently-conjugated M18/2 antibody, before their adoptive transfer into infected *Alox5*$^{-/-}$ mice, and imaged by ISMic. Additionally, *WT* neutrophils were pre-treated with either vehicle (DMSO; same as in Fig. 3F) or 2 μM Nexinhib20, before their adoptive transfer into the recipient. The peripheral Itgb2 redistribution index was determined as described in the Methods section. Data is presented as Means ± SEM N=3 mice for each group. One-way ANOVA analysis using Dunnette's multiple comparison test was used to determine statistical significance.

(D-G) PMNs were pretreated for 20 mins with vehicle (DMSO) or 10 μM GW4869 or 1 μM Nexinhib20 or 10 μM Exo1 and stimulated in the absence or presence of αITGB2 for 15 min with 25 nM fNLFNYK, fixed, stained and imaged by confocal microscopy. Quantification of the extent of F-actin-based cell polarization and cortical NMIIA distribution, internalized ITGB2 and cell adhesion were measured and reported as percentage (D, E & G) or fold change (F) with respect to vehicle controls. Data is presented as mean ± SEM from N=3 independent experiments. One-way ANOVA analysis using Dunnette's multiple comparison test was used to determine statistical significance.

(H) A model depicting the role of the LTB_4-BLT1 axis in promoting neutrophil arrest and extravasation in response to infection *in vivo*. *WT* neutrophils utilize LTB_4 to efficiently redistribute NMIIA and Itgb2 for sustained arrest in the vessels followed by extravasation response to infection. During this process, they release EVs, that relay LTB_4 signals in an autocrine and paracrine manner to augment neutrophil arrest and extravasation behavior. These mechanisms are impaired in *Alox5*$^{-/-}$ neutrophils, which results in their much-reduced arrest and extravasation response to infection.

Supplementary figure legends

Figure S1. Estimate of the GFP-NMIIA redistribution index. Neutrophils purified from GFP-NMIIA mice were treated with either the vehicle (DMSO; top two panel rows) or 5 μM MK886 (bottom two panel rows), injected in infected *Alox5*$^{-/-}$ mice, and imaged in time-lapse modality by ISMic. The optical sections forming the maximal projections shown in Fig.2C were used to quantify the distribution of GFP-NMIIA. White dashed lines indicate vessel boundary and scale bar equals 3 μm. For each time point, each section in Z axis was given a score of 0 or 1 if the GFP-NMIIA was enriched at the center or cortex of an arrested neutrophil manually. An index was generated by averaging the score to the number of stacks analyzed for each neutrophil that displayed arrest behavior during ISMic analysis. For further details please refer the Methods section.

Figure S2. ITGB2 is internalized in a clathrin-independent and dynamin-dependent manner.

(A) PMNs were pre-treated with the vehicle or 2 μM MK886 or 20 μM LY223982 for 20 mins and stimulated with 25 nM fNLFNYK or 250 ng/ml C5a or 250 ng/ml CXCL8 for 15 mins. Adhesion was calculated as described in the Methods section and presented as % to the respective vehicle controls for each chemoattractant. Data is represented as Means ± SEM from N=4 independent experiments. Two-way ANOVA analysis using Dunnette's multiple comparison test was used to determine statistical significance.

(B-C) PMNs were pre-treated with either the vehicle or 20 μM LY223982 for 20 mins. They were incubated with an Alexa488 fluorescently-conjugated antibody against human ITGB2 (αITGB2, CTB104 clone; green) in combination with CellMask Deep Red (magenta) before stimulation with 100 nM fNLFNYK for 10 mins on a fibrinogen-coated surface and acquired as time-lapse 3D imaging using confocal microscopy. **B**- The trajectory of the internalized vesicles was determined as described in the Methods section. Tracks of individual ITGB2-containing vesicles between 5-7 mins post stimulation are over-layed on the maximum intensity projections derived from Z-stacks. See Movie S7. Scale equals 5 μm. **C**- Quantification of the number and distance travelled by ITGB2-containing vesicles for each condition. Data is presented as Means ± SEM from N=3

independent experiments (n=16 cells for vehicle and n=18 cells for LY223982 treatment respectively). Unpaired *t* test with Welch's correction was used to determine statistical significance.

(D-E) PMNs were pre-treated for 20 min with vehicle (DMSO) or the indicated inhibitors of clathrin and dynamin (5 μM PitStop2 or 100 μM MDC or 50 μM Dynasore or 2.5 μM MitMAB), stimulated for 10 min with 25 nM fNLFNYK, fixed and imaged by confocal microscopy. **D**- Representative confocal images of PMNs with internalized ITGB2 under indicated conditions is presented. White dashed lines indicate cell boundary and scale bar equals 5 μm. **E**- The extent of ITGB2 internalization was determined as described in the Method section and the data is presented as % change with respect to the vehicle. Data is represented as mean ± SEM from N=3 independent experiments. One-way ANOVA analysis using Dunnette's multiple comparison test was used to determine statistical significance.

(F) A diagram of the IVM procedure in *Alox5*$^{-/-}$ mouse footpad infection model, where neutrophils from *WT* (labeled green) that were treated as indicated in Figure 5A for 20 mins before being washed, mixed with untreated *Alox5*$^{-/-}$ neutrophils and adoptively transferred into the infected *Alox5*$^{-/-}$ mouse. For further details please refer the Methods section.

Figure S3. A model of ITGB2 trafficking regulated by the LTB_4-BLT1 axis in PMNs. The figure depicts the progression of PMN adhesion on to fibrinogen surface, where in control conditions ITGB2 clusters and migrates to the bottom of the cell to form a ring-like structure, which then disassembles as the PMN begins to migrate. However, upon blockade of LTB4 sensing via BLT1, ITGB2 clusters rapidly internalize and fail to assemble into a ring-like structure at the bottom of the PMN, eventually leading to the deadhesion of PMN from the fibrinogen-coated surface. See Movie S7, Figs. 4D and 4E.

Supplementary movie legends

Movie S1. 2P-IVM of the *LyzM-GFP* mouse footpad at ~1 h post injection of saline in one footpad and heat-killed *E. coli* in the other. Movies are maximum intensity projection of an image stack acquired for a period of ~ 20 mins (min:sec:ff) in each footpad. The vessels were labeled with anti-CD31 (blue). Scale bar equals 50 μm.

Movie S2. 2P-IVM of the footpad in *WT* mouse, that received labeled *WT* neutrophils, at ~1.5 h post injection of saline in one footpad and heat-killed *E. coli* in the other. Movies are maximum intensity projection of an image stack acquired for indicated time periods (min:sec:ff) in each footpad. The vessels were labeled with anti-CD31 (blue). Scale bar equals 50 μm.

Movie S3. 2P-IVM of the *Alox5*$^{-/-}$ mouse footpad at ~1.5 h post infection, where labeled neutrophils (green) were introduced from *WT* or *Alox5*$^{-/-}$ mice. Movies are maximum intensity projection of an image stack acquired for a period of ~ 15-20 mins (min:sec:ff) for each condition. The vessels were labeled with anti-CD31 (blue). Scale bar equals 50 μm.

Movie S4. 2P-IVM of the *Alox5*$^{-/-}$ or *Blt1*$^{-/-}$ mouse footpad at ~1.5 h post infection, where labeled neutrophils (green) were *Blt1*$^{-/-}$ mice. Movies are maximum intensity projection of an image stack acquired for a period of ~ 15-20 mins (min:sec:ff) for each condition. The vessels were labeled with anti-CD31 (blue). Scale bar equals 50 μm.

Movie S5. ISMic imaging of the infected footpad of *Alox5*$^{-/-}$ mouse that received either vehicle or MK886 treated *NMIIA GFP* neutrophils (white), ~1 h post infection. Movies are single slice projection from an image stack and represent ~ 2-4 mins (min:sec:ff) of acquisition for each condition. The vessels were labeled with anti-CD31 (blue). Scale bar equals 3 μm.

Movie S6. ISMic imaging of the infected footpad of *Alox5*$^{-/-}$ mouse that received *WT* or *Alox5*$^{-/-}$ neutrophils labeled for cytoplasm (CellTracker; magenta) and Itgb2 (M18/2; white), ~1 h post infection. Blood vessels are labeled with anti-CD31 (blue). Movies are maximum intensity projection of an image stack acquired for a period of ~ 6-9 mins (min:sec:ff) of acquisition. Scale bar equals 5 μm.

Movie S7. A- Confocal imaging of PMNs stained for plasma membrane (magenta) and αITGB2 (white) that were pre-treated with vehicle (DMSO) or BLT1 inhibitor (LY223982) for 20 mins before stimulation with fNLFNYK and simultaneous live acquisition for 10 mins. Movies are projections of image stacks acquired in 3D, for a period of ~ 10 mins (min:sec:ff). **B**- A view of a section from the cell bottom for the conditions mentioned in A.

Movie S8. 2P-IVM of the footpad at ~2 h post infection, where labeled *WT* neutrophils (green) that were pre-treated with vehicle (DMSO) or the inhibitors MK886 or GW4689 or Nexinhib20 or Exo1 were co-injected with labeled *Alox5*$^{-/-}$ neutrophils (strawberry) into *Alox5*$^{-/-}$ mice. Movies are maximum intensity projection of an image stack acquired for a period of ~ 20-22 mins (min:sec:ff) for each condition. The vessels were labeled with anti-CD31 (blue). Scale bar equals 50 μm.

REFERENCES

1. Liew, P. X. & Kubes, P. The Neutrophil's Role During Health and Disease. *Physiol. Rev.* **99**, 1223–1248 (2019).
2. Lämmermann, T. & Kastenmüller, W. Concepts of GPCR-controlled navigation in the immune system. *Immunol. Rev.* **289**, 205–231 (2019).
3. Subramanian, B. C., Majumdar, R. & Parent, C. A. The role of the LTB4-BLT1 axis in chemotactic gradient sensing and directed leukocyte migration. *Semin. Immunol.* **33**, 16–29 (2017).
4. Zarbock, A. & Ley, K. Mechanisms and consequences of neutrophil interaction with the endothelium. *Am. J. Pathol.* **172**, 1–7 (2008).
5. Majumdar, R., Sixt, M. & Parent, C. A. New paradigms in the establishment and maintenance of gradients during directed cell migration. *Curr. Opin. Cell Biol.* **30**, 33–40 (2014).
6. Werz, O. 5-lipoxygenase: cellular biology and molecular pharmacology. *Curr. Drug Targets Inflamm. Allergy* **1**, 23–44 (2002).
7. Afonso, P. V. *et al.* LTB4 is a signal-relay molecule during neutrophil chemotaxis. *Dev. Cell* **22**, 1079–1091 (2012).
8. Lämmermann, T. *et al.* Neutrophil swarms require LTB4 and integrins at sites of cell death in vivo. *Nature* **498**, 371–375 (2013).
9. Wang, J. *et al.* Visualizing the function and fate of neutrophils in sterile injury and repair. *Science* **358**, 111–116 (2017).
10. David, B. A. & Kubes, P. Exploring the complex role of chemokines and chemoattractants in vivo on leukocyte dynamics. *Immunol. Rev.* **289**, 9–30 (2019).
11. Weigert, R., Porat-Shliom, N. & Amornphimoltham, P. Imaging cell biology in live animals: ready for prime time. *J. Cell Biol.* **201**, 969–979 (2013).
12. Ebrahim, S. & Weigert, R. Intravital microscopy in mammalian multicellular organisms. *Curr. Opin. Cell Biol.* **59**, 97–103 (2019).
13. Faust, N., Varas, F., Kelly, L. M., Heck, S. & Graf, T. Insertion of enhanced green fluorescent protein into the lysozyme gene creates mice with green fluorescent granulocytes and macrophages. *Blood* **96**, 719–726 (2000).
14. Subramanian, B. C., Moissoglu, K. & Parent, C. A. The LTB4-BLT1 axis regulates the polarized trafficking of chemoattractant GPCRs during neutrophil chemotaxis. *J. Cell Sci.* **131**, (2018).
15. Amano, M. *et al.* Phosphorylation and Activation of Myosin by Rho-associated Kinase (Rho-kinase). *J. Biol. Chem.* **271**, 20246–20249 (1996).
16. Milberg, O. *et al.* Concerted actions of distinct nonmuscle myosin II isoforms drive intracellular membrane remodeling in live animals. *J. Cell Biol.* **216**, 1925–1936 (2017).
17. Gillard, J. *et al.* L-663,536 (MK-886) (3-[1-(4-chlorobenzyl)-3-t-butyl-thio-5-isopropylindol-2-yl]-2,2 - dimethylpropanoic acid), a novel, orally active leukotriene biosynthesis inhibitor. *Can. J. Physiol. Pharmacol.* **67**, 456–464 (1989).
18. Riedl, J. *et al.* Lifeact mice for studying F-actin dynamics. *Nat. Methods* **7**, 168–169 (2010).
19. Jackson, W. T., Boyd, R. J., Froelich, L. L., Mallett, B. E. & Gapinski, D. M. Specific inhibition of leukotriene B4-induced neutrophil activation by LY223982. *J. Pharmacol. Exp. Ther.* **263**, 1009–1014 (1992).

20. Fabbri, M. *et al.* Dynamic Partitioning into Lipid Rafts Controls the Endo-Exocytic Cycle of the αL/β2 Integrin, LFA-1, during Leukocyte Chemotaxis. *Mol. Biol. Cell* **16**, 5793–5803 (2005).
21. Majumdar, R., Tavakoli Tameh, A. & Parent, C. A. Exosomes Mediate LTB4 Release during Neutrophil Chemotaxis. *PLoS Biol.* **14**, e1002336 (2016).
22. Johnson, J. L. *et al.* Identification of Neutrophil Exocytosis Inhibitors (Nexinhibs), Small Molecule Inhibitors of Neutrophil Exocytosis and Inflammation: DRUGGABILITY OF THE SMALL GTPase Rab27a. *J. Biol. Chem.* **291**, 25965–25982 (2016).
23. Luberto, C. *et al.* Inhibition of tumor necrosis factor-induced cell death in MCF7 by a novel inhibitor of neutral sphingomyelinase. *J. Biol. Chem.* **277**, 41128–41139 (2002).
24. Feng, Y. *et al.* Exo1: a new chemical inhibitor of the exocytic pathway. *Proc. Natl. Acad. Sci. U. S. A.* **100**, 6469–6474 (2003).
25. Tanaka, Y., Adams, D. H. & Shaw, S. Proteoglycans on endothelial cells present adhesion-inducing cytokines to leukocytes. *Immunol. Today* **14**, 111–115 (1993).
26. Springer, T. A. Traffic signals on endothelium for lymphocyte recirculation and leukocyte emigration. *Annu. Rev. Physiol.* **57**, 827–872 (1995).
27. Miyabe, Y. *et al.* Complement C5a Receptor is the Key Initiator of Neutrophil Adhesion Igniting Immune Complex-induced Arthritis. *Sci. Immunol.* **2**, (2017).
28. Grespan, R. *et al.* CXCR2-specific chemokines mediate leukotriene B4-dependent recruitment of neutrophils to inflamed joints in mice with antigen-induced arthritis. *Arthritis Rheum.* **58**, 2030–2040 (2008).
29. Girbl, T. *et al.* Distinct Compartmentalization of the Chemokines CXCL1 and CXCL2 and the Atypical Receptor ACKR1 Determine Discrete Stages of Neutrophil Diapedesis. *Immunity* **49**, 1062-1076.e6 (2018).
30. Genschmer, K. R. *et al.* Activated PMN Exosomes: Pathogenic Entities Causing Matrix Destruction and Disease in the Lung. *Cell* **176**, 113-126.e15 (2019).
31. Wculek, S. K. & Malanchi, I. Neutrophils support lung colonization of metastasis-initiating breast cancer cells. *Nature* **528**, 413–417 (2015).
32. Xu, J. *et al.* Divergent signals and cytoskeletal assemblies regulate self-organizing polarity in neutrophils. *Cell* **114**, 201–214 (2003).
33. Vicente-Manzanares, M., Choi, C. K. & Horwitz, A. R. Integrins in cell migration – the actin connection. *J. Cell Sci.* **122**, 199–206 (2009).
34. Anderson, D. C. & Springer, T. A. Leukocyte adhesion deficiency: an inherited defect in the Mac-1, LFA-1, and p150,95 glycoproteins. *Annu. Rev. Med.* **38**, 175–194 (1987).
35. Shaw, S. K. *et al.* Coordinated Redistribution of Leukocyte LFA-1 and Endothelial Cell ICAM-1 Accompany Neutrophil Transmigration. *J. Exp. Med.* **200**, 1571–1580 (2004).
36. Masedunskas, A. & Weigert, R. Intravital two-photon microscopy for studying the uptake and trafficking of fluorescently conjugated molecules in live rodents. *Traffic Cph. Den.* **9**, 1801–1810 (2008).
37. Shitara, A. *et al.* Cdc42 negatively regulates endocytosis during apical membrane maintenance in live animals. *Mol. Biol. Cell* **30**, 324–332 (2019).
38. Morin, N. A. *et al.* Nonmuscle myosin heavy chain IIA mediates integrin LFA-1 de-adhesion during T lymphocyte migration. *J. Exp. Med.* **205**, 195–205 (2008).

39. Hind, L. E., Vincent, W. J. B. & Huttenlocher, A. Leading from the Back: The Role of the Uropod in Neutrophil Polarization and Migration. *Dev. Cell* **38**, 161–169 (2016).
40. Stanley, P., Tooze, S. & Hogg, N. A role for Rap2 in recycling the extended conformation of LFA-1 during T cell migration. *Biol. Open* **1**, 1161–1168 (2012).
41. Riggs, K. A. *et al.* Regulation of integrin endocytic recycling and chemotactic cell migration by syntaxin 6 and VAMP3 interaction. *J. Cell Sci.* **125**, 3827–3839 (2012).
42. Swamydas, M., Luo, Y., Dorf, M. E. & Lionakis, M. S. ISOLATION OF MOUSE NEUTROPHILS. *Curr. Protoc. Immunol. Ed. John E Coligan Al* **110**, 3.20.1-3.20.15 (2015).
43. Brown, L. G. A Survey of Image Registration Techniques. *ACM Comput Surv* **24**, 325–376 (1992).
44. Chen, D. *et al.* Machine learning based methodology to identify cell shape phenotypes associated with microenvironmental cues. *Biomaterials* **104**, 104–118 (2016).
45. Xu, C. & Prince, J. L. Snakes, shapes, and gradient vector flow. *IEEE Trans. Image Process. Publ. IEEE Signal Process. Soc.* **7**, 359–369 (1998).

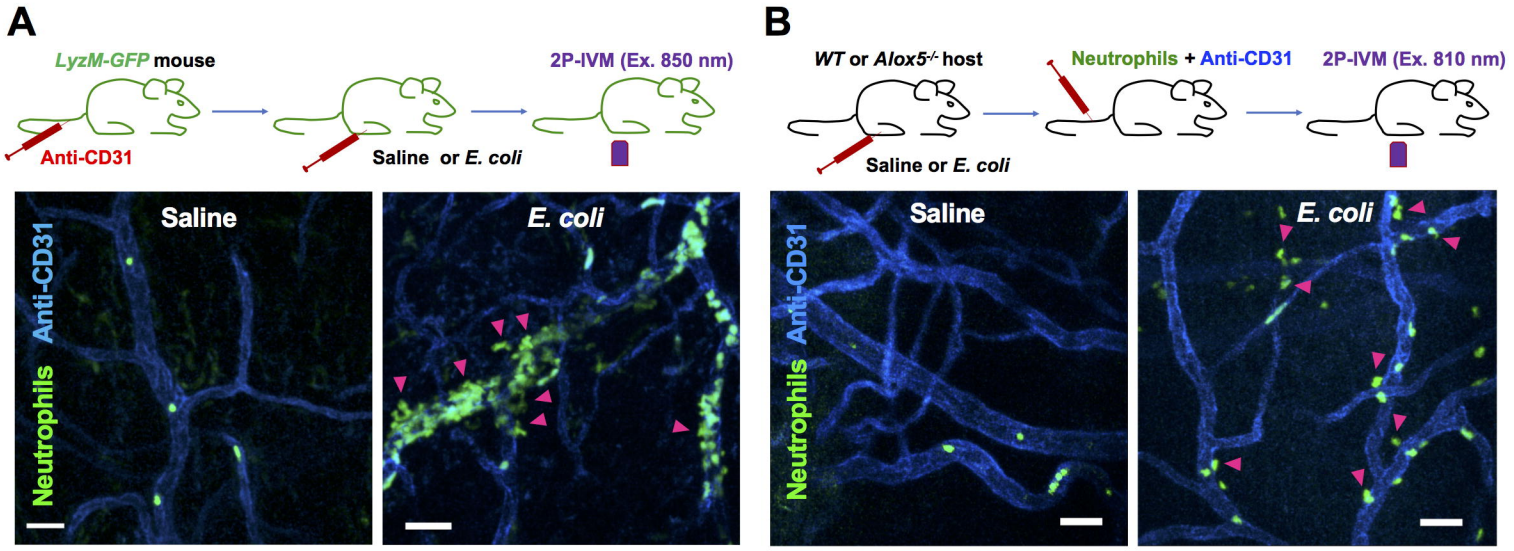
A
LyzM-GFP mouse
Anti-CD31
Saline or E. coli
2P-IVM (Ex. 850 nm)
Saline
E. coli
Neutrophils
Anti-CD31
B
WT or Alox5-/- host
Saline or E. coli
Neutrophils + Anti-CD31
2P-IVM (Ex. 810 nm)
Saline
E. coli
Neutrophils
Anti-CD31

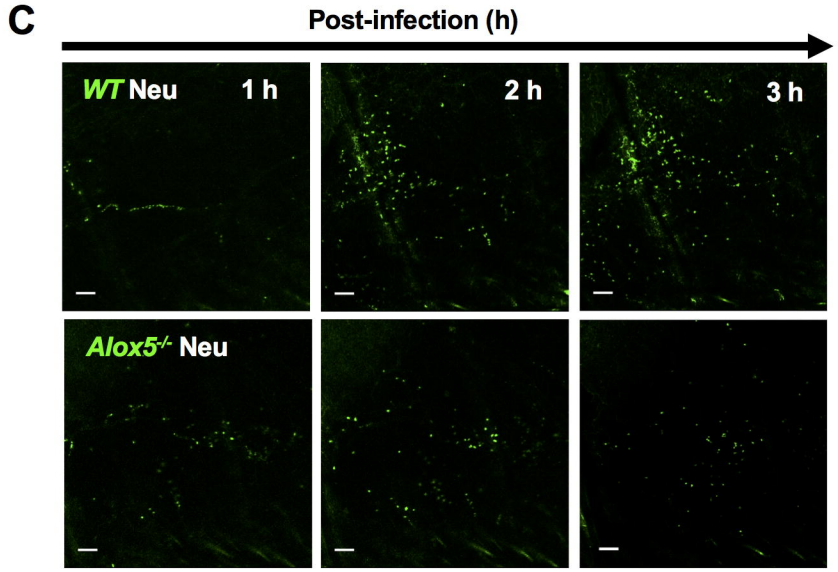
C
Post-infection (h)
WT Neu
1 h
2 h
3 h
Alox5-/- Neu

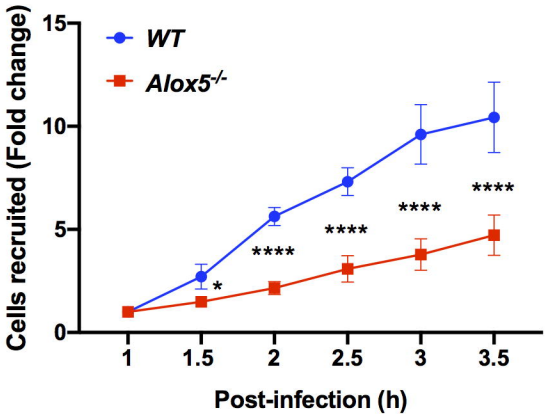
D
WT
Alox5-/-
Cells recruited (Fold change)
Post-infection (h)
0
5
10
15
1
1.5
2
2.5
3
3.5
*
****
****
****
****

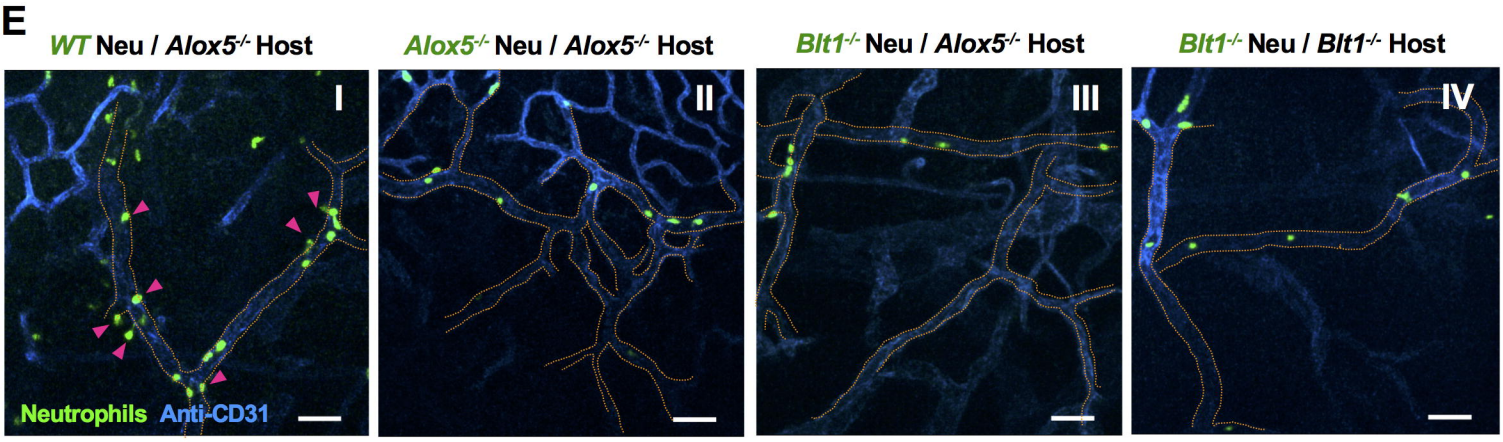
E
WT Neu / Alox5-/- Host
Alox5-/- Neu / Alox5-/- Host
Blt1-/- Neu / Alox5-/- Host
Blt1-/- Neu / Blt1-/- Host
I
II
III
IV
Neutrophils
Anti-CD31

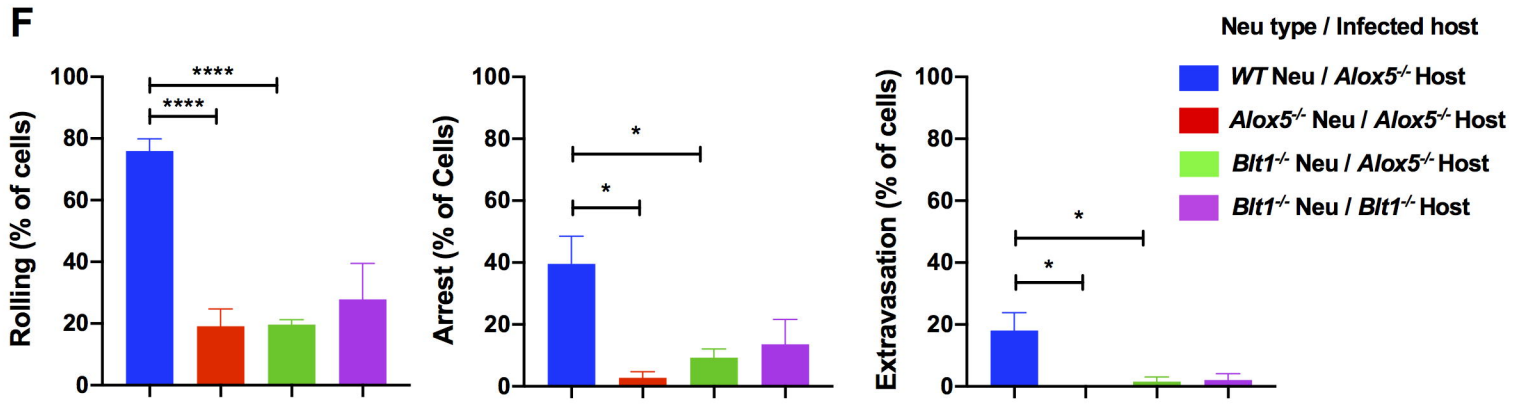
F
Rolling (% of cells)
Arrest (% of Cells)
Extravasation (% of cells)
0
20
40
60
80
100
****
****
*
*
*
*
Neu type / Infected host
WT Neu / Alox5-/- Host
Alox5-/- Neu / Alox5-/- Host
Blt1-/- Neu / Alox5-/- Host
Blt1-/- Neu / Blt1-/- Host

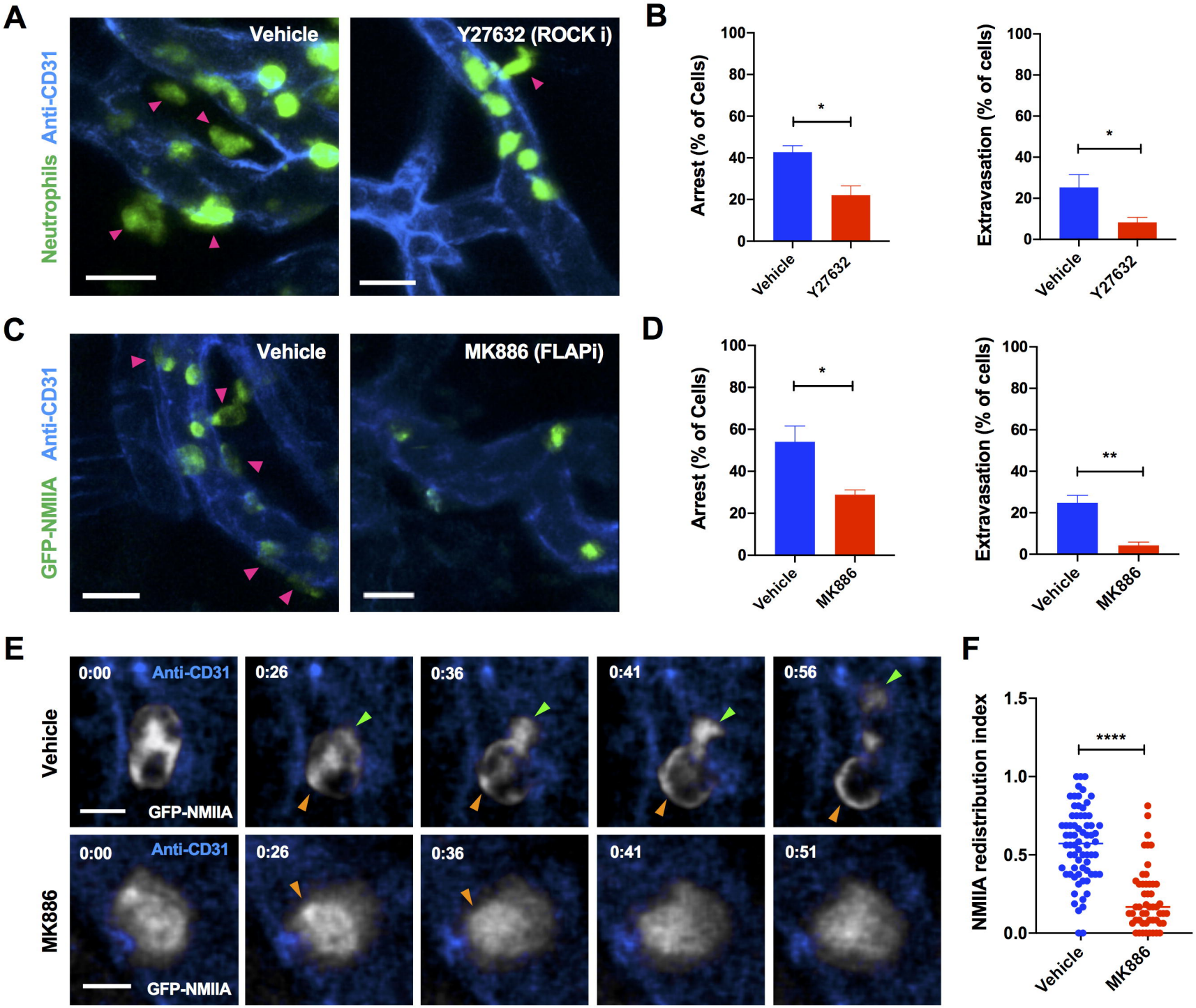
A
Neutrophils Anti-CD31
Vehicle
Y27632 (ROCK i)
B
Arrest (% of Cells)
Extravasation (% of cells)
Vehicle
Y27632
C
GFP-NMIIA Anti-CD31
Vehicle
MK886 (FLAPi)
D
Arrest (% of Cells)
Extravasation (% of cells)
Vehicle
MK886
E
Vehicle
MK886
Anti-CD31
GFP-NMIIA
0:00
0:26
0:36
0:41
0:56
0:51
F
NMIIA redistribution index
Vehicle
MK886

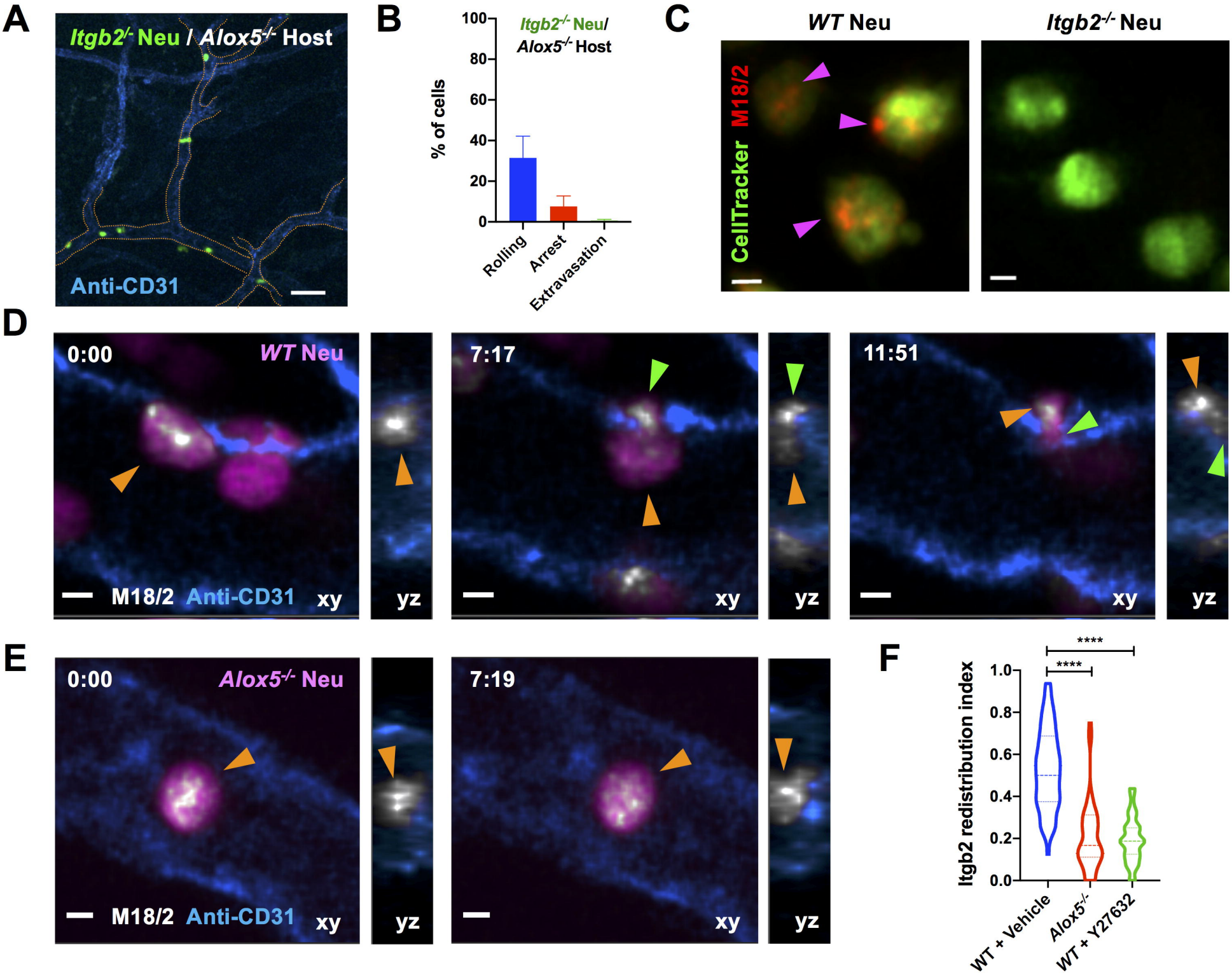
A
Itgb2-/- Neu / Alox5-/- Host
Anti-CD31
B
Itgb2-/- Neu/
Alox5-/- Host
% of cells
100
80
60
40
20
0
Rolling
Arrest
Extravasation
C
WT Neu
Itgb2-/- Neu
CellTracker M18/2
D
0:00
WT Neu
M18/2 Anti-CD31
xy
yz
7:17
11:51
E
0:00
Alox5-/- Neu
7:19
F
Itgb2 redistribution index
1.0
0.8
0.6
0.4
0.2
0.0
****
****
WT + Vehicle
Alox5-/-
WT + Y27632

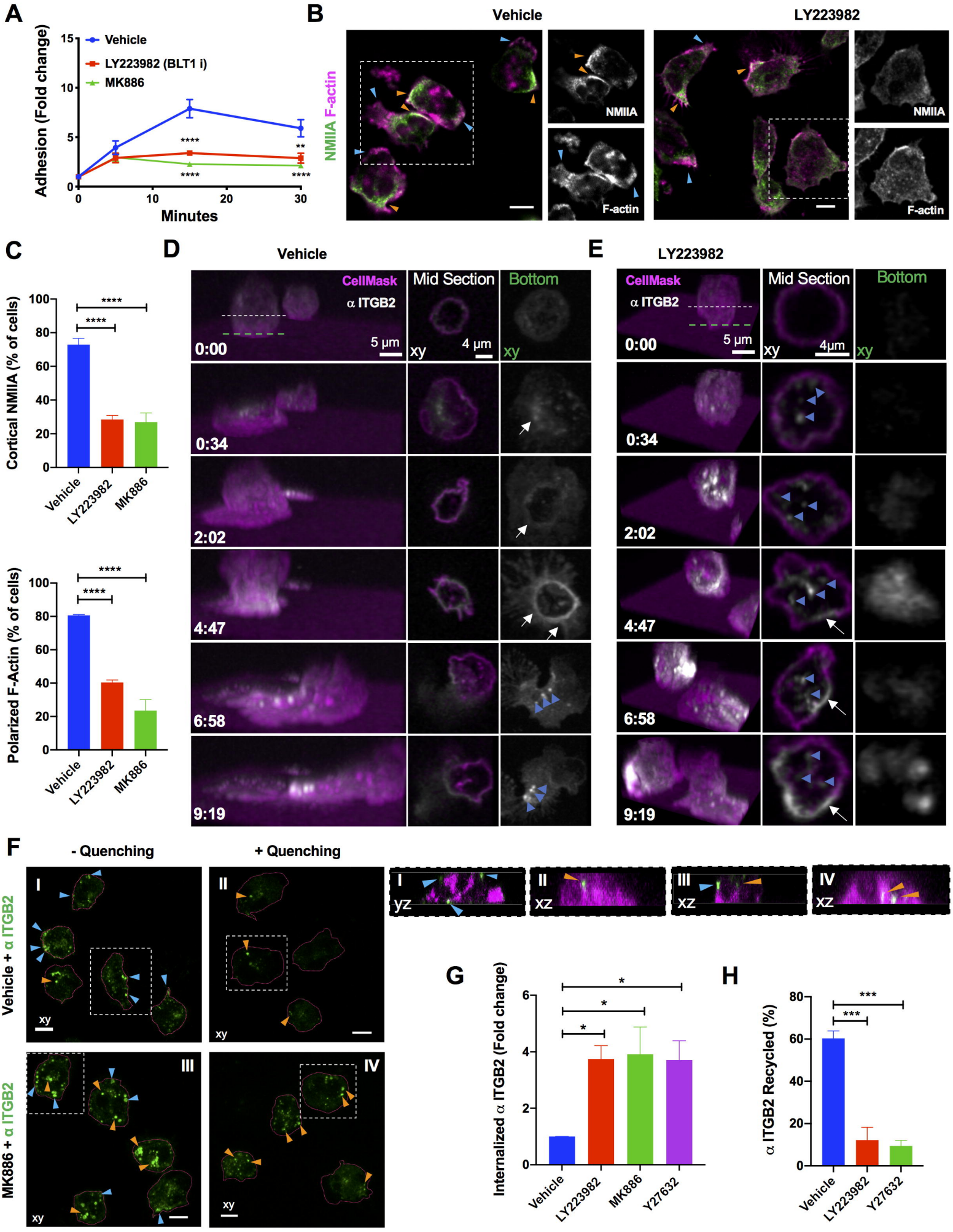
A
Adhesion (Fold change)
Vehicle
LY223982 (BLT1 i)
MK886
Minutes
B
Vehicle
LY223982
NMIIA F-actin
NMIIA
F-actin
C
Cortical NMIIA (% of cells)
Polarized F-Actin (% of cells)
Vehicle
LY223982
MK886
D
Vehicle
CellMask
α ITGB2
Mid Section
Bottom
5 µm
4 µm
xy
0:00
0:34
2:02
4:47
6:58
9:19
E
LY223982
4µm
F
- Quenching
+ Quenching
Vehicle + α ITGB2
MK886 + α ITGB2
I
II
III
IV
yz
xz
G
Internalized α ITGB2 (Fold change)
Y27632
H
α ITGB2 Recycled (%)

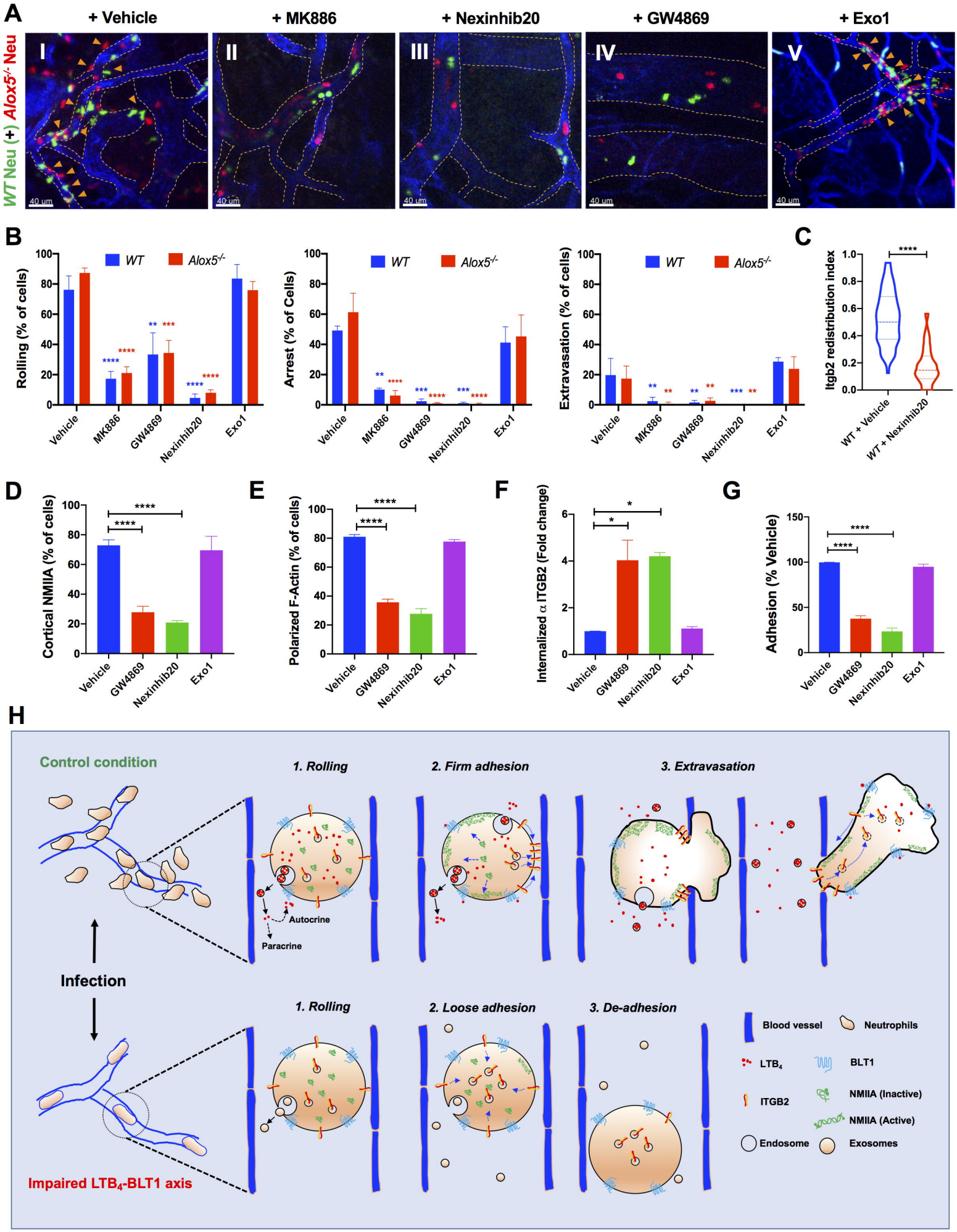
A
+ Vehicle
+ MK886
+ Nexinhib20
+ GW4869
+ Exo1
WT Neu (+) Alox5-/- Neu
I
II
III
IV
V
40 um
B
Rolling (% of cells)
Arrest (% of Cells)
Extravasation (% of cells)
WT
Alox5-/-
Vehicle
MK886
GW4869
Nexinhib20
Exo1
C
Itgb2 redistribution index
WT + Vehicle
WT + Nexinhib20
D
Cortical NMIIA (% of cells)
E
Polarized F-Actin (% of cells)
F
Internalized α ITGB2 (Fold change)
G
Adhesion (% Vehicle)
H
Control condition
1. Rolling
2. Firm adhesion
3. Extravasation
Autocrine
Paracrine
Infection
1. Rolling
2. Loose adhesion
3. De-adhesion
Impaired LTB4-BLT1 axis
Blood vessel
Neutrophils
LTB4
BLT1
ITGB2
NMIIA (Inactive)
NMIIA (Active)
Endosome
Exosomes